J. Am. Soc. Mass Spectrom. (2016) 27:2064–2070
DOI: 10.1007/s13361-016-1498-6

RESEARCH ARTICLE

Localization of Post-Translational Modifications in Peptide Mixtures via High-Resolution Differential Ion Mobility Separations Followed by Electron Transfer Dissociation

Matthew A. Baird, Alexandre A. Shvartsburg

Department of Chemistry, Wichita State University, 1845 Fairmount, Wichita, KS 67260-0051, USA

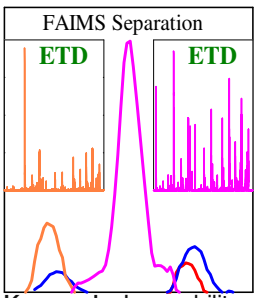

Abstract. Precise localization of post-translational modifications (PTMs) on proteins and peptides is an outstanding challenge in proteomics. While electron transfer dissociation (ETD) has dramatically advanced PTM analyses, mixtures of localization variants that commonly coexist in cells often require prior separation. Although differential or field asymmetric waveform ion mobility spectrometry (FAIMS) achieves broad variant resolution, the need for standards to identify the features has limited the utility of approach. Here we demonstrate full a priori characterization of variant mixtures by high-resolution FAIMS coupled to ETD and the procedures to systematically extract the FAIMS spectra for all variants from such data.

Keywords: Ion mobility spectrometry, FAIMS, Electron transfer dissociation, PTM localization

Received: 6 May 2016/Revised: 28 August 2016/Accepted: 31 August 2016/Published Online: 19 September 2016

Introduction

Many proteins incorporate post-translational modifications (PTMs) that govern critical biological functions [1, 2]. For example, the phosphorylation pattern of human τ protein is thought to control the aggregation of paired helical filaments in Alzheimer's disease by influencing the *cis/trans* ratio of prolyl bonds adjacent to T^{231} and S^{235} and thereby the protein conformation [3]. Phosphorylated sites also have distinct regulatory functions for non-amyloid proteins, such as ERK and CDK family members and adapter proteins like SRC and Fak [4]. The same PTMs often attach in different locations on the backbone, creating "localization variants" that coexist in vivo and have different and even opposite biological activities [5–8]. For instance, demethylation of H3 histone is associated with transcription activation when on the K4 residue but with heterochromatin and repression when on the closest lysine (K9) [6].

As the technologies for identifying and quantifying primary protein sequences mature, the proteomics frontier is moving to the characterization of PTMs and their roles in disease states [1, 2, 9]. That advance is hindered by the open-ended diversity of PTMs (with hundreds discovered to date) and substoichiometric modification [9]. Many PTMs are labile, including perhaps the most biologically consequential—the phosphorylation considered here [2, 5, 7, 8, 10]. Ergodic methods such as collision-induced dissociation (CID) usually eject them from the peptide and/or shift them to another residue before severing the backbone, obliterating or falsifying the attachment site information [2, 10]. Thus, comprehensive tandem mass spectrometry (MS/MS) analysis of PTMs requires a direct fragmentation mechanism, such as the electron capture dissociation (ECD) or electron transfer dissociation (ETD) that cut the peptide backbone at every residue without abstracting PTMs [2, 5, 11, 12]. However, MS/MS methods are fundamentally unable to distinguish some variants in a mixture of three or more due to the absence of unique product masses [12]. This can in theory be overcome by subsequent fragmentations, but (unlike with CID in MS^n protocols) successive ETD application is impractical in view of (1) charge reduction in the first step, which produces few or no multiply charged ions that could be precursors for the second step, and (2) low ETD yield into each fragment (normally ~0.1%–1% because of limited ETD efficiency and nonspecific dissociation along ~10–100 channels).

Hence, peptide variants generally need to be separated prior to the MS/MS step. While proteolytic digests are routinely fractionated by liquid chromatography (LC) prior to MS/MS, it often fails to resolve the localization variants, especially those

Electronic supplementary material The online version of this article (doi:10.1007/s13361-016-1498-6) contains supplementary material, which is available to authorized users.

Correspondence to: Alexandre A. Shvartsburg;
e-mail: alexandre.shvartsburg@wichita.edu

with nearby alternatively occupied sites that also produce the most similar fragmentation patterns [7, 13].

A growing substitute to LC is ion mobility spectrometry (IMS), where ionized compounds are driven through gas by electric field and fractionated depending on the transport properties [14]. The original approach of linear IMS is based on the absolute ion mobility (K) at moderate fields and achieves resolving powers (R) up to ~200 in the drift tube (DT) [15, 16] and ~50 in the traveling-wave (TW) [17] implementations. These techniques can partly separate the phospho-peptide and unmodified peptide domains and resolve some variants [18–20]. Unfortunately, those could not be assigned using ETD: the extended times needed for a suitable yield of reaction between the ions and ETD reagent (commonly ~100–300 ms) greatly exceed the temporal peak width of ion packets upon IMS separation (typically ~0.1–1 ms) and thus implementing ETD on the fly after dispersive DT or TW IMS separations would obliterate the established resolution. Whereas the IMS resolving power can be augmented somewhat using the cyclotron paradigm [21] to pull apart the variants better, that would counteract matching the IMS peak width and the ETD timescale.

A newer approach of differential or field asymmetric waveform IMS (FAIMS) leverages the nonlinear ion motion in fields of high intensity (E) to sort ions by the mean derivative of $K(E)$ function over a certain range [22, 23]. That quantity is elicited employing an asymmetric waveform of some amplitude (dispersion voltage, DV) set up across a gap between two electrodes, through which ions are carried by the gas flow. Ions injected into the gap are pushed to either electrode, but a given species can be balanced (and thus pass and be detected) by superposing a particular fixed compensation voltage (CV) on the waveform. Scanning CV, commonly expressed as the compensation field (E_C) to normalize for the gap width, reveals the spectrum of species present. As the $K(E)$ derivative is correlated to ion mass substantially weaker than the mobility itself, FAIMS is much more orthogonal to MS than linear IMS [24–26]. The gain depends on the analyte nature and is about 4-fold for peptides [27]. Hence, FAIMS tends to resolve isomers finer than linear IMS with equal R metric.

The resolution in FAIMS strongly depends on the gap shape, maximizing in planar gaps where homogeneous electric field allows equilibrating only one species at a time [28], and the gas composition. The He/N_2 buffers generally work well because of higher ion mobilities in lighter gases and prominent non-Blanc effect in mixtures of molecules with disparate masses [23, 29]. The optimized buffers and high-fidelity waveform generators have recently raised the attainable R up to ~500 for multiply charged peptides [30]. That performance has allowed fully separating all variants tried so far for sequences up to ~3 kDa, including those with smaller PTMs such as acetylation and methylation [31, 32]. Those experiments utilized an ion trap MS system without ETD capability, and the spectral annotation relied on pure standards. With real protein digests, synthesizing those for all potentially relevant variants is often prohibitive.

Rather, one wishes to identify the features disentangled by FAIMS via ETD. That has been shown and utilized in proteomic analyses, but the commercial cylindrical-gap FAIMS device provided only marginal variant separation [12, 33–35]. Here we describe a new high-resolution FAIMS/ETD platform and deploy it to fully resolve a mixture of PTM localization variants and assign all a priori.

Experimental

Methods

Our FAIMS/MS platform is an upgrade on the earlier instrument [30]. The custom planar FAIMS unit stays as reported, with the gap width of 1.88 mm and length of ~50 mm. The bisinusoidal waveform with the 2:1 harmonics ratio and DV = 4 kV is delivered by a generator (Heartland Mobility, Bothell, WA, USA) protected from arc discharge to permit operation near the breakdown threshold without risking equipment damage. The electrospray (ESI) emitter is biased at ~3 kV above the curtain plate of FAIMS inlet.

That system is mounted on a Thermo LTQ XL ion trap with ETD capability, enabling ETD of species filtered by FAIMS. A major present challenge for high-resolution FAIMS/ETD analyses is low sensitivity due to poor ion utilization in both stages. We have ameliorated that problem by effective FAIMS/MS coupling via an electrodynamic ion funnel interface preceded by a slit aperture that maximizes the overlap with ion beams exiting the FAIMS gap [28].

For the ETD stage, the temperatures were 160°C at the source, transfer line, and restrictor, and 110°C at the reagent (fluoranthene) vial. The pressure of chemical ionization gas (He) was delivered to the mass spectrometer at 10 PSI. Under those conditions, the reagent ion signal was ~10^6. During ETD, we scanned CV at the rate of 0.5 V/min to acquire the E_C spectra or kept it constant to obtain the fragmentation pattern for a given feature. Most ETD spectra were obtained with the 120–140 ms reaction time followed by supplemental collisional activation at the potential of 25 V, which has balanced the sensitivity with coverage. All fragments were singly charged.

The N_2 and He/N_2 buffers were formulated from UHP components by digital flow meters (MKS Instruments, Andover, MA, USA) controlled from a PC, purified by an Agilent filter (RMSHY-4), and delivered at the "standard" rate of 2 L/min. This pilot study targets the τ 226–240 segment (VAVVRT^{231}PPKS^{235}PS^{237}S^{238}AK) monophosphorylated on T^{231} (**1**), S^{235} (**2**), S^{237} (**3**), or S^{238} (**4**) with the monoisotopic mass of $m = 1602.9$ Da previously separated by FAIMS [31]. Their equimolar mixtures (~5 μM each) were dissolved in 50:49:1 water/methanol/acetic acid and infused to the emitter at ~0.5 uL/min. This peptide set was chosen for the inordinate difficulty for differentiation by MS/MS ensuing from the two prolines between T^{231} and S^{235}, one proline between S^{235} and S^{237}, and adjacent S^{237} and S^{238} residues. As the C-

terminal side of proline is protected from cleavage, the fragments differ by just two pairs for **1** and **2** and one pair for **2** and **3**, or **3** and **4**.

Results and Discussion

These peptides turn into protonated ions with the charge states (z) of 2 ($m/z = 802.5$) and 3 ($m/z = 535.3$), but both FAIMS separation and ETD tend to work much better for $z = 3$ [31]. Possible c- and z-fragments for all four variants (with either $z =$ 2 or 3) needed to extract the E_C spectra were cataloged using Protein Prospector and compared to identify the unique m/z values (Table 1) [36]. We start from the N_2 buffer and add He in steps to improve resolution. We first look at a binary mixture (**1** + **2**) without the problem of non-unique fragments, then employ FAIMS to unlock that problem for the quaternary mixture. Crucially, the second step uses no findings for the binary mixture.

The E_C spectrum of (**1** + **2**) in N_2 has two major features, and the ETD pattern of 3+ precursor comprises all unique fragments (UF) for **1** (c_8 at m/z of 917.5, c_9 at 1045.6, z_6 at 560.3, and z_7 at 688.4) and **2** (c_8 at 837.5, c_9 at 965.6, z_6 at 640.2, and z_7 at 768.3), as well as numerous nondistinguishing products (Figure 1a). All four UF for either variant have identical spectra, but those for **1** and **2** drastically differ (Figure 1b, c). This illustrates the self-consistency and resolution of our procedure to extract the spectra for peptide variants from those for UF. The spectrum for each precursor is reconstructed by aggregating those for all four fragments (Figure 1d): **1** is readily separated from **2**, but not vice versa because the higher-E_C peak (features **1 B**–**D**) almost coincides with **2**. The sum of two traces matches the measured total spectrum (that also includes all nondistinguishing fragments), further confirming the protocol.

In He/N_2 buffers, the E_C spectra for four UF of either **1** or **2** remain close and their reconstructed traces also sum to the measured spectrum (Supplementary Figures S1, S2). Upon He addition, the **1D** feature rapidly disappears while the minor **1B** and **1C** grow between the major peaks **1A** and **2C** (Figure 2). The evolution of **2** is simpler: the front ledge (**2A** and **2B**) vanishes. The variant separation becomes perfect by ~30% He.

With the approach validated, we progress to the mixture of all four variants. Besides all ETD products in Figure 1, we see (Figure 3a) the distinguishing fragments at $m/z = 1149.7$ (c_{11}), 369.1 (z_4), and 456.2 (z_5). The c_{12} fragment ($m/z = 1236.7$) was observed, but swamped by undetermined interference. Therefore, the only marker for **4** was the weak z_4 feature.

The lack of UF for **2** and **3** can be overcome by accounting for both presence and absence of specific products at particular FAIMS features and exploiting the experimental trace to properly scale the E_C spectra for various variants and their combinations elicited from ETD data. [As the yields of different c/z pairs are grossly unequal (Figure 3a), the heights of raw E_C spectra correlate with the precursor abundances only weakly).

The E_C spectrum in N_2 contains three major peaks (Figure 3). We first use UF to find the spectrum for **1** (Figure 3b), which naturally copies that in Figure 1. The set **2/3/4** has four UF (c_8, c_9, z_6, z_7) that sum to the spectrum overlapping with peaks B and C, but not A. Hence A must be solely due to **1**, and we can scale the trace for **1** to fit that peak in the measured spectrum (Figure 3c). The spectrum for **1/2** obtained from UF c_{11} (1229.7) and z_4 (376.2) has the dominant peak coinciding with C but little intensity at B, and the opposite nearly holds for the spectrum for **3/4** derived from parallel UF at 1149.7 and 456.2 (Figure 3b). That allows us to scale the spectrum for **3/4** to fit B, then subtract it from the measured trace to scale the spectrum for **1/2** to fit C (Figure 3c). We finally subtract from that the spectrum for **1** to deduce the one for **2**. The normalized spectrum for **4** is extracted from its sole UF (Figure 3b). Whereas the lack of a pronounced feature in the measured trace at its peak position precludes robust scaling and, thus, subtraction from the spectrum for **3/4**, clearly B is due to **3** rather than **4**. The sum of spectra for **1**, **2**, and **3/4** reasonably tracks the measured trace (Figure 3c). Overall, FAIMS has fractionated a

Table 1. Theoretically Expected ETD Fragments of the τ 226–240 Peptides Monophosphorylated at T^{231}, S^{235}, S^{237}, or S^{238}

		C Fragments						Z Fragments			
		T231	S235	S237	S238			T231	S235	S237	S238
V	1	117.10	117.10	117.10	117.10	V	15	–	–	–	–
A	2	188.14	188.14	188.14	188.14	A	14	1488.77	1488.77	1488.77	1488.77
V	3	287.21	287.21	287.21	287.21	V	13	1417.73	1417.73	1417.73	1417.73
V	4	386.28	386.28	386.28	386.28	V	12	1318.66	1318.66	1318.66	1318.66
R	5	542.38	542.38	542.38	542.38	R	11	1219.60	1219.60	1219.60	1219.60
T	6	–	–	–	–	T	10	1063.49	1063.49	1063.49	1063.49
P	7	–	–	–	–	P	9	–	–	–	–
P	8	917.50	837.53	837.53	837.53	P	8	–	–	–	–
K	9	1045.59	965.63	965.63	965.63	K	7	688.38	768.34	768.34	768.34
S	10	–	–	–	–	S	6	560.28	640.25	640.25	640.25
P	11	1229.68	1229.68	1149.71	1149.71	P	5	–	–	–	–
S	12	1316.71	1316.71	1316.71	1236.74	S	4	376.20	376.20	456.16	456.16
S	13	1403.74	1403.74	1403.74	1403.74	S	3	289.16	289.16	289.16	369.13
A	14	1474.78	1474.78	1474.78	1474.78	A	2	202.13	202.13	202.13	202.13
K	15	–	–	–	–	K	1	131.09	131.09	131.09	131.09

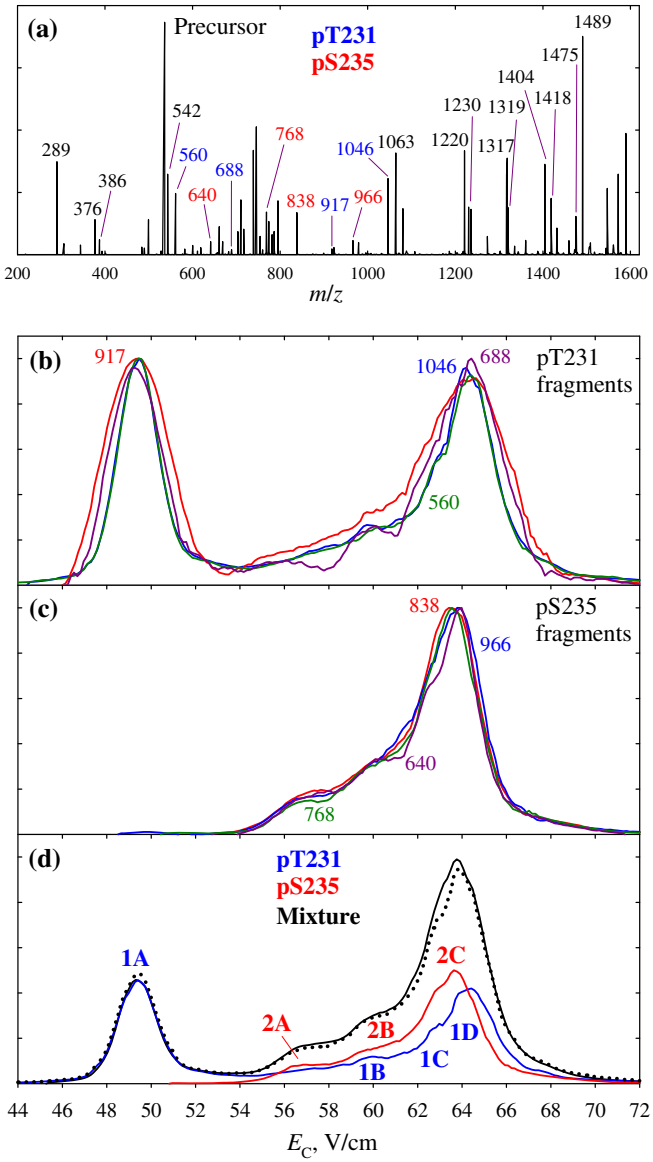

Figure 1. FAIMS/ETD data (with N_2 buffer) for the pT^{231}/pS^{235} mixture: **(a)** total ETD spectrum with *c*/*z* fragments labeled (unique fragments color-coded); **(b)**, **(c)** normalized spectra for all UF of pT^{231} and pS^{235} with the *m*/*z* values as marked; **(d)** measured trace (line) with the scaled spectra for both species produced by summing the spectra for all UF of each (above), and the mixture spectrum reconstructed by adding the two (dotted line)

mixture of four components into A (**1**), B (predominately **3** + **4**), and C (mostly **1** + **2**). This partial separation is nearly enough for full characterization using ETD, which can deal with binary mixtures as explained above.

Much higher resolution is available with He/N_2 buffers. By 30% He, the three peaks separate nearly baseline, with B featuring a shoulder B1 on the left and tail B3 on the right (Figure 4a). The trace is interpreted via the outlined process (Supplementary Figure S4): the spectra for **1** and **2/3/4** indicate that A consists exclusively of **1**. As the spectrum for **1/2** has a peak at C but those for **1** and **3/4** do not overlap with C, it must be solely due to **2**. Thus, the spectra for **1** and **1/2** can be accurately scaled, and **2** recovered by subtracting **1** from **1/2**. The spectrum for **3/4** again peaks at B and is scaled to it (the spectrum for **1/2** hardly overlaps with B). The peak for **4** has moved to the low-E_C side of B, where it engenders B1. It can now be scaled by subtracting the spectrum for **1/2/3**, obtained from UF c_{12} (1316.7) and z_3 (289.2) and scaled to fit B, from the trace in the appropriate region. The spectrum for **3** is derived by subtracting the scaled spectra for **2** and **4** from that for **2/3/4**. Within the logic of the above solutions, one can alter the details. For example, in the last step, one can instead subtract the spectrum for **1/2** from **1/2/3**. These variations do not affect the outcome. Again, the spectra for all four variants add up to the measured trace.

The separation further improves at 40% He (Figure 4b). Here, the structures B1 and B3 split into well-defined peaks. Analysis along the above path (Supplementary Figure S5) tells that B1 comprises **4** (which continues transposing to lower E_C relative to **3**) with some **1**, while B3 is made from **1** and some **2**. This conclusion agrees with the results for (**1** + **2**) mixture in Figure 2.

The fraction of He in FAIMS is limited by electrical breakdown, presently to under ~65% (v/v). However, a common constraint for peptides is that some disappear largely or completely upon He addition, presumably upon "self-cleaning" where the species that changed the CV by more than the baseline peak width upon isomerization inside the gap are filtered out [37]. This can occur in any medium, but is more probable at greater He concentrations because of both stronger heating and higher resolution that decrease the magnitude of geometry shift needed for elimination. Accordingly, the best variant separations were often achieved at He fractions significantly below the breakdown threshold, such as ~40%–60% [32]. The ion counts required for MS/MS and especially ETD exceed those for MS detection. This shifts the resolution/sensitivity balance toward the latter, and the optimum He fractions for FAIMS/ETD are lower than those for FAIMS/MS: here ~30%–40%. Although the specific number will vary depending on the instrument and sample, the preference for lower fractions of He or H_2 in FAIMS/MS/MS relative to FAIMS/MS analyses of same species would persist.

Multiple features in E_C spectra exhibited by most variants, especially with the N_2 buffer (Figure 3), correspond to 3-D conformers ubiquitous for unmodified peptides of similar size (e.g., bradykinin or syntide 2) in IMS and FAIMS analyses [38–40]. These interfere with the variant resolution for modified peptides by competing for finite separation space. More stringent "self-cleaning" at higher He fractions often reduces the conformational diversity by eliminating less stable geometries [37] like in overtone mobility spectrometry [41], which improves the variant separation beyond the straightforward increase of resolving power due to the expansion of separation space and narrowing of individual peaks (Figure 4).

For maximum signal, all above mass spectra were collected in the "turbo mode" with low MS resolving power. That sufficed for the present exemplary mixture, but many realistic

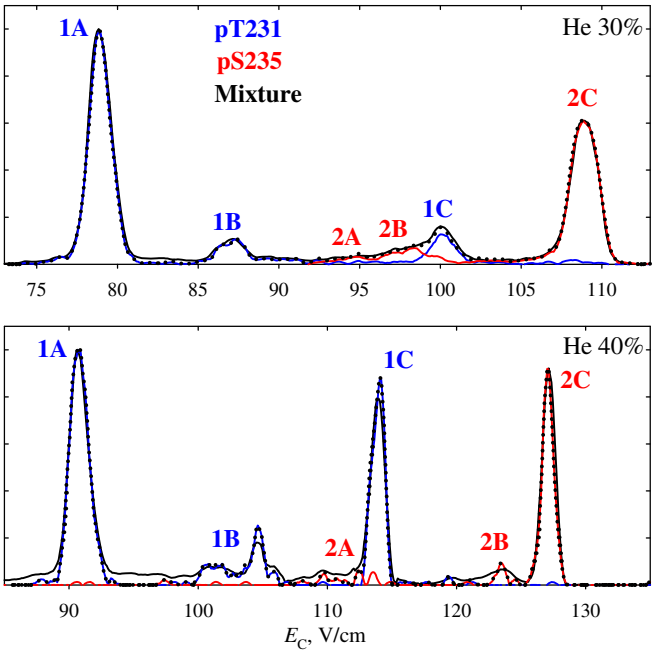

Figure 2. Same as Figure 1d with He/N_2 buffers

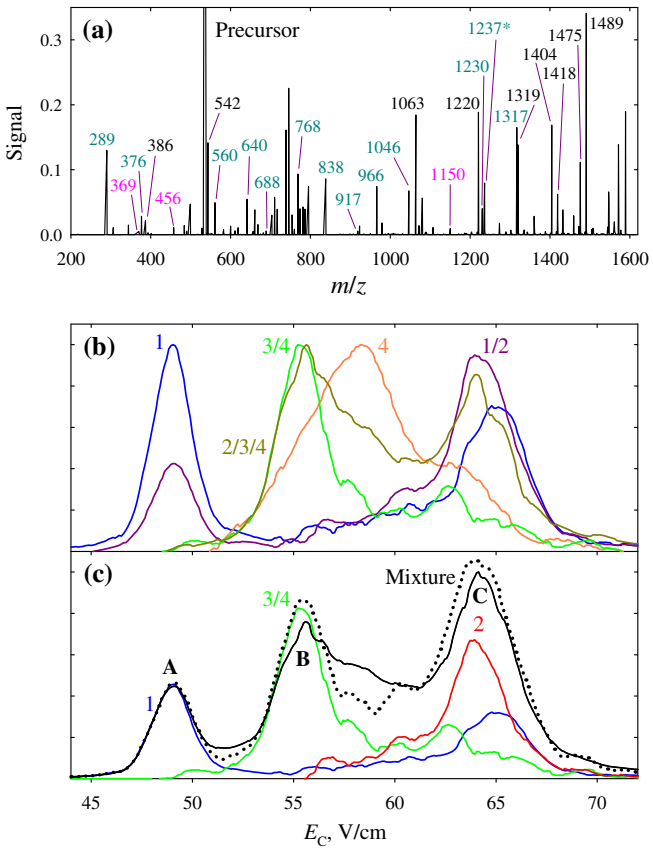

Figure 3. FAIMS/ETD data (with N_2 buffer) for the four-variant mixture: **(a)** total ETD spectrum with *c*/*z* fragments labeled; **(b)** normalized spectra for the precursors or their groups derived by summing the spectra for all distinguishing fragments; **(c)** measured trace (line) with the scaled spectra for individual species derived from above data, and the mixture spectrum obtained by adding them all (dotted line)

samples require higher MS resolution and mass accuracy. Those can be reached in the mode resembling multiple reaction monitoring (MRM), where the CV during ETD is switched between discrete spectral peaks selected from the initial MS-only scan. This permits extended data accumulation at a given E_C that compensates for lower signal (even at the highest He fractions) at least in the "normal" MS mode (Figure 5). For one, that enables baseline resolution of the c_{12} informative and z_{12} noninformative fragments partly merged in the turbo mode.

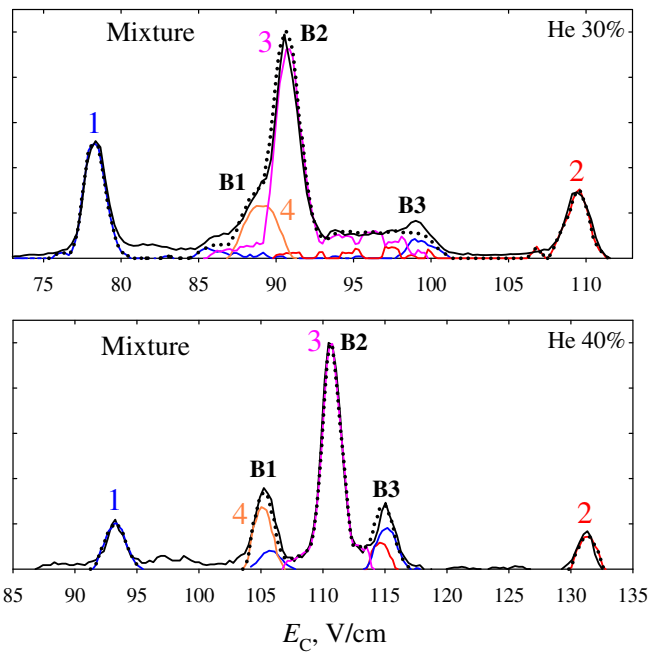

Figure 4. Same as Figure 3c with He/N_2 buffers

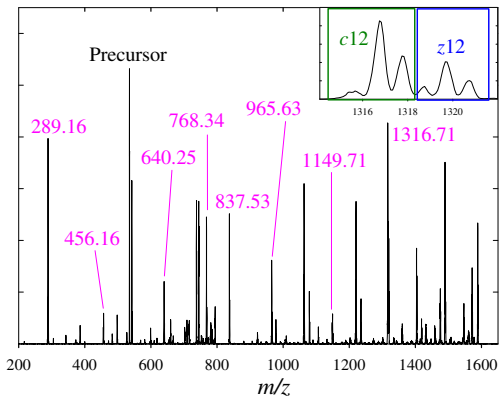

Figure 5. ETD spectrum measured at the peak B2 of Figure 4b in the normal mode

Alternatively, this MRM-like mode lowers the detection limits for all variants.

These peptides are also somewhat separated by FAIMS for $z = 2$ [31]. However, ETD of the 2+ ions from quaternary mixture produced no fragments below $m/z = 1220$ despite the reaction time up to 350 ms (Figure 6). This has limited the UF to c_{11} and c_{12} that would not elucidate the picture even had FAIMS resolved all the variants. Hence, we did not apply FAIMS/ETD to 2+ ions. However, those may help for other peptides that exhibit more informative fragments (e.g., because of PTMs closer to either terminus that would turn large-mass ions into UF) and/or better separation in the 2+ state.

An important concern is the reproducibility of results over time and between instruments and laboratories. Here, we used the peptide stock solutions made for work at PNNL [31] and kept since – partly not in a freezer and through multiple freezing/thawing cycles. Yet present variant separations derived from ETD fragments (Figure 4) are close to those obtained using standards in 2011 [31]. Hence, the conformational distinctions between variants responsible for observed FAIMS resolution are conserved in solution over lengthy storage times and wide

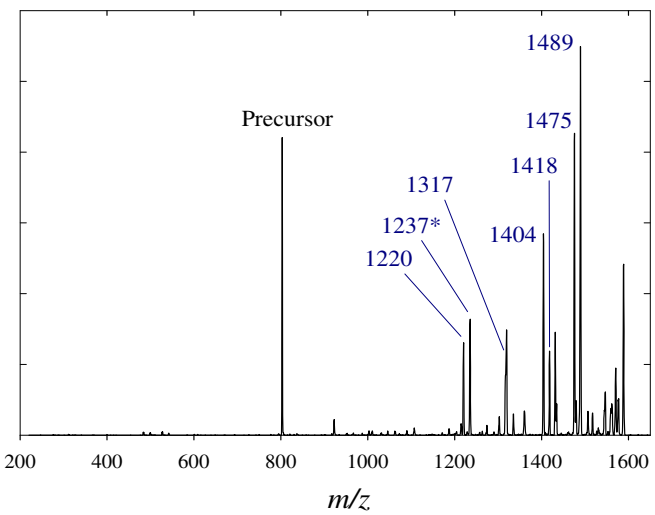

Figure 6. ETD spectrum of the four-variant mixture (selecting 2+ precursors)

temperature ranges and/or (more likely) immaterial to analyses in the current regime where unfolding upon strong field heating [37, 42] largely erases the memory of solution structure. Either way, the consistent outcome after such a long time and on different FAIMS and MS systems in another lab shows the stability of approach. A related issue is the influence of solution composition. The E_C spectra for present variants were independent of the solvent pH in the range of ~2–3 relevant to typical LC conditions, also suggesting the destruction of solution conformations in FAIMS [31].

Although this work was for singly modified peptides, variants involving multiple PTMs were resolved by FAIMS equally well [31, 32] and would likewise be subject to instant approach. Real-world mixtures generally involve uneven variant concentrations. However, the ion signals for present individual standards without FAIMS vastly differed because of unequal ESI ionization efficiency. In FAIMS/ETD experiments, these differences were convoluted with those in FAIMS transmission efficiency, total ETD yield, and fragment partitioning to produce quite different feature intensities for different variants (e.g., Figure 4). However, all variants including **4** with a very weak (unscaled) peak were confidently identified. With these convolutions, characterizing samples with unequal variant amounts may be harder or easier, depending on which variant is enhanced.

Conclusions

We have integrated the highest-resolution FAIMS system with ETD (on an ion trap) and demonstrated the ability of a new platform to fully characterize the mixtures of peptide localization variants not amenable to ETD alone because of the lack of unique fragments (UF). The key aspects of data interpretation are the (1) summation of counts for all UF of each variant, (2) scaling of so-reconstructed precursor spectra to the measured trace, and (3) use of the variant groups that have UF, the information regarding both present and missing fragments, and signal subtraction to derive the spectra for each variant. The approach was carefully validated for a benchmark mixture of four variants (including two with adjacent alternative PTM sites) previously characterized using standards [31]. However, it is not limited to four peptides given the facility of ETD to deal with binary mixtures and the flexibility of FAIMS separations controlled by changing the dispersion voltage and gas composition. Real bioanalyses would benefit from higher mass resolution and accuracy, and we are working to couple high-resolution FAIMS to Orbitrap mass spectrometers with ETD capability. The present combination of high-resolution FAIMS with ETD can also be extended to other MS/MS methods.

Acknowledgments

The authors thank Gordon A. Anderson (GAACE) and Dr. Keqi Tang (PNNL) for aid with instrumental development, and Andrew Bowman and Julia Kaszycki for experimental assistance. This research was funded by NIH K-INBRE (P20 GM103418),

NSF First (EPS-0903806), and NSF CAREER (CHE-1552640). A.A.S. also holds a faculty appointment at the Moscow Engineering Physics Institute (Russia) and has interest in Heartland Mobility, LLC that produces FAIMS systems and ion funnel interfaces such as those utilized in this work.

References

1. Mann, M., Jensen, O.N.: Proteomic analysis of post-translational modifications. Nat. Biotechnol. **21**, 255–261 (2003)
2. Molina, H., Horn, D.M., Tang, N., Mathivanan, S., Pandey, A.: Global proteomic profiling of phosphopeptides using electron transfer dissociation tandem mass spectrometry. Proc. Natl. Acad. Sci. U. S. A. **104**, 2199–2204 (2007)
3. Daly, N.L., Hoffmann, R., Otvos, L., Craik, D.J.: Role of phosphorylation in the conformation of tau peptides implicated in Alzheimer's disease. Biochemistry **39**, 9039–9046 (2000)
4. Nebreda, A.R.: CDK Activation by non-cyclin proteins. Current Opin. Cell Biol. **18**, 192–198 (2006)
5. Chi, A., Huttenhower, C., Geer, L.Y., Coon, J.J., Syka, J.E.P., Bai, D.L., Shabanowitz, J., Burke, D.J., Troyanskaya, O.G., Hunt, D.F.: Analysis of phosphorylation sites on proteins from *Saccharomyces cerevisiae* by electron transfer dissociation (ETD) mass spectrometry. Proc. Natl. Acad. Sci. U.S.A. **104**, 2193–2198 (2007)
6. Mosammaparast, N., Shi, Y.: Reversal of histone methylation: biochemical and molecular mechanisms of histone demethylases. Annu. Rev. Biochem. **79**, 155–179 (2010)
7. Langlais, P., Mandarino, L.J., Yi, Z.: Label-free relative quantification of co-eluting isobaric phosphopeptides of insulin receptor substrate-1 by HPLC-ESIMS/MS. J. Am. Soc. Mass Spectrom. **21**, 1490–1499 (2010)
8. Cunningham, D.L., Sweet, S.M.M., Cooper, H.J., Heath, J.K.: Differential phosphoproteomics of fibroblast growth factor signaling: identification of Src family kinase-mediated phosphorylation events. J. Proteome Res. **9**, 2317–2328 (2010)
9. Savitski, M.M., Nielsen, M.L., Zubarev, R.A.: ModifiComb, a new proteomic tool for mapping substoichiometric post-translational modifications, finding novel types of modifications, and fingerprinting complex protein mixtures. Mol. Cell. Proteom. **5**, 935–948 (2006)
10. Palumbo, A., Reid, G.E.: Evaluation of gas-phase rearrangement and competing fragmentation reactions on protein phosphorylation site assignment using collision induced dissociation-MS/MS and MS3. Anal. Chem. **80**, 9735–9743 (2008)
11. Swaney, D.L., McAlister, G.C., Wirtala, M., Schwartz, J.C., Syka, J.E.P., Coon, J.J.: Supplemental activation method for high-efficiency electron-transfer dissociation of doubly protonated peptide precursors. Anal. Chem. **79**, 477–485 (2007)
12. Xuan, Y., Creese, A.J., Horner, J.A., Cooper, H.J.: High-field asymmetric waveform ion mobility spectrometry (FAIMS) coupled with high-resolution electron transfer dissociation mass spectrometry for the analysis of isobaric phosphopeptides. Rapid Commun. Mass Spectrom. **23**, 1963–1969 (2009)
13. Singer, D., Kuhlmann, J., Muschket, M., Hoffman, R.: Separation of multiphosphorylated peptide isomers by hydrophilic interaction chromatography on an aminopropyl phase. Anal. Chem. **82**, 6409–6414 (2010)
14. Eiceman, G.A., Karpas, Z., Hill, H.H.: Ion mobility spectrometry, 3rd edn. CRC Press, Boca Raton (2014)
15. Dugourd, P.H., Hudgins, R.R., Clemmer, D.E., Jarrold, M.F.: High-resolution ion mobility measurements. Rev. Sci. Instrum. **68**, 1122–1129 (1997)
16. Srebalus, C.A., Li, J., Marshall, W.S., Clemmer, D.E.: Gas-phase separations of electrosprayed peptide libraries. Anal. Chem. **71**, 3918–3927 (1999)
17. Pringle, S.D., Giles, K., Wildgoose, J.L., Williams, J.P., Slade, S.E., Thalassinos, K., Bateman, R.H., Bowers, M.T., Scrivens, J.H.: An investigation of the mobility separation of some peptide and protein ions using a new hybrid quadrupole/traveling wave IMS/oa-ToF instrument. Int. J. Mass Spectrom. **261**, 1–12 (2007)
18. Ruotolo, B.T., Verbeck, G.F., Thomson, L.M., Woods, A.S., Gillig, K.J., Russell, D.H.: Distinguishing between phosphorylated and nonphosphorylated peptides with ion mobility-mass spectrometry. J. Proteome Res. **1**, 303–306 (2002)
19. Glover, M.S., Dilger, J.M., Acton, M.D., Arnold, R.J., Radivojac, P., Clemmer, D.E.: Examining the influence of phosphorylation on peptide ion structure by ion mobility spectrometry-mass spectrometry. J. Am. Soc. Mass Spectrom. **27**, 786–794 (2016)
20. Ibrahim, Y., Shvartsburg, A.A., Smith, R.D., Belov, M.E.: Ultrasensitive identification of localization variants of modified peptides using ion mobility spectrometry. Anal. Chem. **83**, 5617–5623 (2011)
21. Merenbloom, S.I., Glaskin, R.S., Henson, Z.B., Clemmer, D.E.: High-resolution ion cyclotron mobility spectrometry. Anal. Chem. **81**, 1482–1487 (2009)
22. Guevremont, R.J.: High-field asymmetric waveform ion mobility spectrometry: a new tool for mass spectrometry. J. Chromatogr. A **1058**, 3–19 (2004)
23. Shvartsburg, A.A.: Differential ion mobility spectrometry. CRC Press, Boca Raton (2008)
24. Guevremont, R., Barnett, D.A., Purves, R.W., Vandermey, J.: Analysis of a tryptic digest of pig hemoglobin using ESI-FAIMS-MS. Anal. Chem. **72**, 4577–4584 (2000)
25. Shvartsburg, A.A., Mashkevich, S.V., Smith, R.D.: Feasibility of higher-order differential ion mobility separations using new asymmetric waveforms. J. Phys. Chem. A **110**, 2663–2673 (2006)
26. Shvartsburg, A.A., Isaac, G., Leveque, N., Smith, R.D., Metz, T.O.: Separation and classification of lipids using differential ion mobility spectrometry. J. Am. Soc. Mass Spectrom. **22**, 1146–1155 (2011)
27. Shvartsburg, A.A., Creese, A.J., Smith, R.D., Cooper, H.J.: Separation of a set of peptide sequence isomers using differential ion mobility spectrometry. Anal. Chem. **83**, 6918–6923 (2011)
28. Shvartsburg, A.A., Li, F., Tang, K., Smith, R.D.: High-resolution field asymmetric waveform ion mobility spectrometry using new planar geometry analyzers. Anal. Chem. **78**, 3706–3714 (2006)
29. Shvartsburg, A.A., Tang, K., Smith, R.D.: Understanding and designing field asymmetric waveform ion mobility spectrometry separations in gas mixtures. Anal. Chem. **76**, 7366–7374 (2004)
30. Shvartsburg, A.A., Seim, T.A., Danielson, W.F., Norheim, R., Moore, R.J., Anderson, G.A., Smith, R.D.: High-definition differential ion mobility spectrometry with resolving power up to 500. J. Am. Soc. Mass Spectrom. **24**, 109–114 (2013)
31. Shvartsburg, A.A., Singer, D., Smith, R.D., Hoffman, R.: Ion mobility separation of isomeric phosphopeptides from a protein with variant modification of adjacent residues. Anal. Chem. **83**, 5078–5085 (2011)
32. Shvartsburg, A.A., Zheng, Y., Smith, R.D., Kelleher, N.L.: Separation of variant methylated histone tails by differential ion mobility. Anal. Chem. **84**, 6317–6320 (2012)
33. Bridon, G., Bonneil, E., Muratore-Schroeder, T., Caron-Lizotte, O., Thibault, P.: Improvement of phosphoproteome analyses using FAIMS and decision tree fragmentation. Application to the insulin signaling pathway in *Drosophila melanogaster* S2 cells. J. Proteome Res. **11**, 927–940 (2012)
34. Creese, A.J., Cooper, H.J.: Separation and identification of isomeric glycopeptides by high field asymmetric waveform ion mobility spectrometry. Anal. Chem. **84**, 2597–2601 (2012)
35. Ulasi, G.N., Creese, A.J., Hui, S.X., Penn, C.W., Cooper, H.J.: Comprehensive mapping of O-glycosylation in flagellin from *Campylobacter jejuni* 11168: a multi-enzyme differential ion mobility mass spectrometry approach. Proteomics **15**, 2733–2745 (2015)
36. Protein Prospector available at: http://prospector.ucsf.edu/prospector/mshome.htm. Accessed June 2015
37. Shvartsburg, A.A., Li, F., Tang, K., Smith, R.D.: Distortion of ion structures by field asymmetric waveform ion mobility spectrometry. Anal. Chem. **79**, 1523–1528 (2007)
38. Pierson, N.A., Chen, L., Valentine, S.J., Russell, D.H., Clemmer, D.E.: Number of solution states of bradykinin from ion mobility and mass spectrometry measurements. J. Am. Chem. Soc. **133**, 13810–13813 (2011)
39. Purves, R.W., Barnett, D.A., Ells, B., Guevremont, R.: Gas-phase conformers of the $[M+2H]^{2+}$ ion of bradykinin investigated by combining high-field asymmetric waveform ion mobility spectrometry, hydrogen/deuterium exchange, and energy-loss measurements. Rapid Commun. Mass Spectrom. **15**, 1453–1456 (2001)
40. Shvartsburg, A.A., Danielson, W.F., Smith, R.D.: High-resolution differential ion mobility separations using He-rich gases. Anal. Chem. **82**, 2456–2462 (2010)
41. Lee, S., Ewing, M.A., Nachtigall, F.M., Kurulugama, R.T., Valentine, S.J., Clemmer, D.E.: Determination of cross sections by overtone mobility spectrometry: evidence for loss of unstable structures at higher overtones. J. Phys. Chem. B **114**, 12406–12415 (2010)
42. Robinson, E.W., Shvartsburg, A.A., Tang, K., Smith, R.D.: Control of ion distortion in field asymmetric waveform ion mobility spectrometry via variation of dispersion field and gas temperature. Anal. Chem. **80**, 7508–7515 (2008)